Journal of Thermal Science Vol.29, No.3 (2020) 609–622

https://doi.org/10.1007/s11630-020-1169-6 **Article ID: 1003-2169(2020)03-0609-14**

A Multiple-Relaxation-Time Lattice Boltzmann Model for Natural Convection in a Hydrodynamically and Thermally Anisotropic Porous Medium under Local Thermal Non-Equilibrium Conditions

YANG Bo[1], WU Wei[2,*], LI Maodong[1], ZHAI Wei[1]

1. Guangzhou Special Pressure Equipment Inspection and Research Institute, Guangzhou 510663, China
2. School of Chemistry and Chemical Engineering, South China University of Technology, Guangzhou 510640, China

Abstract: To investigate the natural convective process in a hydrodynamically and thermally anisotropic porous medium at the representative elementary volume (REV) scale, the present work presented a multiple-relaxation-time lattice Boltzmann method (MRT-LBM) based on the assumption of local thermal non-equilibrium conditions (LTNE). Three sets of distribution function were used to solve the coupled momentum and heat transfer equations. One set was used to compute the flow field based on the generalized non-Darcy model; the other two sets were used to solve the temperature fields of fluid and solid under the LTNE. To describe the anisotropy of flow field of the porous media, a permeability tensor and a Forchheimer coefficient tensor were introduced into the model. Additionally, a heat conductivity tensor and a special relaxation matrix with some off-diagonal elements were selected for the thermal anisotropy. Furthermore, by selecting an appropriate equilibrium moments and discrete source terms accounting for the local thermal non-equilibrium effect, as well as choosing an off-diagonal relaxation matrix with some specific elements, the presented model can recover the exact governing equations for natural convection under LTNE with anisotropic permeability and thermal conductivity with no deviation terms through the Chapman-Enskog procedure. Finally, the proposed model was adopted to simulate several benchmark problems. Good agreements with results in the available literatures can be achieved, which indicate the wide practicability and the good accuracy of the present model.

Keywords: lattice Boltzmann method, natural convection in anisotropic porous medium, local thermal non-equilibrium

1. Introduction

Natural convection in the porous media has been extensively studied, owing to the widespread applications in many fields of science and engineering, such as geothermal energy systems, underground spread of pollutants in soils, petroleum reservoir modelling, and electronic management with porous media. In order to further analysis the performance of such systems, it is of considerable interest to predict the convectional fluid flow and temperature distribution of the porous media. In the literatures, there exist two major models for the natural convection in porous media. The first and most commonly employed one is the local thermal equilibrium (LTE) model, which assumes that the saturating fluid and the constituent porous solid matrix are at the same

Received: Oct 24, 2018 Corresponding author: WU Wei E-mail: dawuweijun@163.com

temperature. However, the assumption of LTE will induce substantial error in cases of certain applications, such as the case with a significant internal heat generation in fluid phase or solid matrix, or the case with a very large difference in thermal conductivity between the solid and fluid, and so on. In these cases, the rate of temperature change for the fluid and solid will be no longer equal and thus the assumption of LTE will be broken down [1]. Thus, the local thermal non-equilibrium (LTNE) model, which assumes that there exists a finite temperature difference between the solid and the fluid phases leading to the heat transfer between these two phases, must be adopted in these applications. In the LTNE models, two energy equations with appropriate coupling term accounted for the interfacial heat transfer are usually adopted to model the temperature fields of the fluid and solid phases, respectively [2]. In the past two decades, many numerical simulations based on the well-developed traditional methods (e.g. finite difference method (FDM) and finite volume method (FVM)) have been conducted to investigate the natural convection in porous media under LTNE condition [3].

As a promising numerical tool for computational fluid dynamics, the lattice Boltzmann method (LBM), which is based on the kinetic theory and the discretization of the mesoscopic kinetic equations, has been successfully adopted to study the heat transfer and fluid flow in porous media, owing to its numerous advantages [4–6]. By introducing some additional terms into the LB equation to account for the drag force due to the presence of the porous media, Guo and Zhao [7] developed a generalized LB model for the incompressible flow in porous media at the representative elementary volume (REV) scale. Then, they further extended the generalized LB model to study the natural convection heat transfer in the porous media with double distribution function LB model [8]. Gao and Chen [9] proposed a thermal LB model to investigate the natural convection in the porous media at the REV scale under the LTE condition. Wang et al. [10] also proposed a modified LBGK model for convection heat transfer in porous media under the LTE condition, in which the macroscopic equations can be correctly recovered by constructing a modified equilibrium distribution function and the corresponding source term. However, all of the above-mentioned LB models employ the Bhatnagar-Gross-Krook (BGK) collision model, which encounters some defects, such as numerical instability at low viscosities. In order to overcome these defects of LBGK models, Liu et al. [11] established a multiple-relaxation-time (MRT) LB model for simulating convection heat transfer in porous media, in which the porosity of the porous media is introduced into the equilibrium moments and force terms in the moment space. Very recently, Hu et al. [12] proposed a MRT-LB model for simulating flow and heat transfer in the hydrodynamically and thermally anisotropic porous medium at the REV scale under LTE condition. In their model, the correct Darcy-Brinkman-Forchheimer and energy equations with anisotropic permeability and thermal conductivity can be recovered through the Chapman-Enskog procedure by selecting the appropriate equilibrium distributions, relaxation matrix and discrete force/heat source terms.

It can be found from the above literatures review that most REV-LB models for natural convection in porous media are based on the LTE assumptions. Gao and Chen [13] further extended the model to account for the non-local thermodynamic equilibrium (non-LTE) condition with two new distribution functions for the temperature fields of the fluid and solid matrix phases. It should be noted that in most of the existing REV-LB models for porous media, deviation term exists in the corresponding macroscopic equations when the velocity vector varies with space or time through the Chapman-Enskog analysis, which has significant influence on numerical error. Furthermore, there is no LB model for flow and heat transfer problems in the anisotropic porous medium under LTNE condition, which are very important due to its wide range of applications. Thus, the aim of the present paper is to develop a MRT-LB model to model the natural convection in a hydrodynamically and thermally anisotropic porous medium under LTNE. For this purpose, through an appropriate selection of the equilibrium moments, discrete source terms and an off-diagonal relaxation matrix, the proposed MRT-LB model can recover the governing equations under LTNE with anisotropic permeability and thermal conductivity with no deviation terms through the Chapman-Enskog procedure.

2. Problem Description & Governing Equations

The schematic of the physical model for the natural convective flow and heat transfer in a 2D cavity filled with a fluid-saturated porous medium is shown in Fig. 1. The side length of the cavity is L. To derive the governing equations, the following simplifying assumptions are particularly made: (1) the flow is incompressible and laminar; (2) the solid matrix of the porous media is in local thermal non-equilibrium (LTNE) state with the fluid; (3) the thermos-physical properties of the fluid as well as of the porous matrix are constant except for density dependency of the buoyancy term in the momentum equation, which follows Boussinesq approximation; (4) the viscous dissipation and radiative heat transfer can be neglected; (5) the porous medium is anisotropic in permeability and the solid matrix is anisotropic in thermal conductivity; (6) the generalized non-Darcy model is used to depict the drag force due to the presence of porous medium. Based on these assumptions, the detailed volume-averaged governing

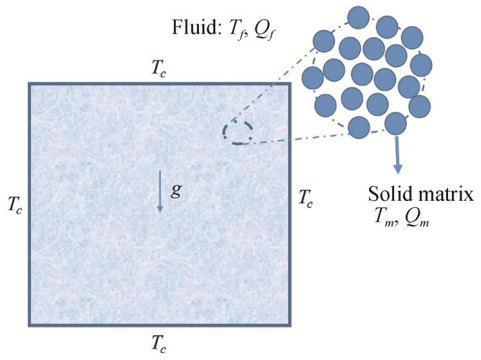

Fig. 1 The schematic of the physical model

equations for the natural convective flow and heat transfer in a 2D cavity filled with a fluid-saturated porous medium at the REV scale can be derived as follows:

Continuity equation:

$$\nabla \cdot \boldsymbol{u} = 0 \tag{1a}$$

Momentum equation:

$$\frac{\partial \boldsymbol{u}}{\partial t} + \nabla \cdot \left(\frac{\boldsymbol{u}\boldsymbol{u}}{\varepsilon} \right) = -\frac{1}{\rho_f} \nabla (\varepsilon p) + \nu_e \nabla^2 \boldsymbol{u} + \boldsymbol{F}_b \tag{1b}$$

Energy equation for fluid:

$$\varepsilon \frac{\partial T_f}{\partial t} + \nabla \cdot (\boldsymbol{u} T_f) = \nabla \cdot \left(\frac{\boldsymbol{\kappa}_{ef}}{(\rho c_p)_f} \nabla T_f \right) + \frac{h(T_m - T_f) + \varepsilon Q_f}{(\rho c_p)_f} \tag{1c}$$

Energy equation for solid matrix:

$$(1-\varepsilon) \frac{\partial T_m}{\partial t} = \nabla \cdot \left(\frac{\boldsymbol{\kappa}_{em}}{(\rho c_p)_m} \nabla T_m \right) + \frac{h(T_f - T_m) + (1-\varepsilon) Q_m}{(\rho c_p)_m} \tag{1d}$$

where, ρ is the density of the fluid; $\boldsymbol{u}$ and p are the volume-averaged velocity and pressure respectively; ε is the porosity of the porous media; ν_e is the effective kinematic viscosity; c_p is the specific heat; $\boldsymbol{\kappa}_e$ is the second-order tensor for the effective conductivity; Q is the volumetric internal heat source; T is the temperature; the subscripts "m" and "f" denote the solid matrix and the fluid respectively. $\boldsymbol{F}_b$ represents the total body force induced by the presence of a porous medium and other external force fields, and can be given by:

$$\boldsymbol{F}_b = -\varepsilon \nu_f \boldsymbol{K}^{-1} \boldsymbol{u} - \varepsilon \boldsymbol{C}_{\boldsymbol{F}} |\boldsymbol{u}| \boldsymbol{u} + \varepsilon \boldsymbol{G} \tag{2}$$

where, $\boldsymbol{K}$ and $\boldsymbol{C}_{\boldsymbol{F}}$ are the second-order tensors for the intrinsic permeability of the porous media and the Forchheimer coefficient respectively; $|\boldsymbol{u}|$ is the magnitude of the superficial velocity; ν_f is the viscosity of the fluid which is related, but not necessarily equal to ν_e. The first and the second terms on the right side of Eq. (2) denote the linear viscous and non-linear inertial drag forces due to the presence of the porous media, respectively. The buoyancy force $\boldsymbol{G}$ induced by the gravitational force can be given by the Boussinesq approximation:

$$\boldsymbol{G} = \boldsymbol{g} \beta_T (T_f - T_{ref}) \tag{3}$$

where $\boldsymbol{g}$ is the gravity acceleration vector; β_T is the thermal expansion coefficient; T_{ref} is the reference temperature.

The anisotropic porous medium is assumed to be hydrodynamically and thermally anisotropic. The hydrodynamic anisotropy can be represented based on both permeability and Forchheimer coefficient tensor, while thermal anisotropy of the solid matrix can be depicted by the thermal conductivity tensor. The principal permeabilities are K_1 and K_2, respectively. The angle between K_1 direction and x-direction is θ_p. Then the permeability tensor K can be given by the following matrix:

$$\boldsymbol{K} = \begin{bmatrix} K_1 \cos^2 \theta_p + K_2 \sin^2 \theta_p & (K_1 - K_2) \sin \theta_p \cos \theta_p \\ (K_1 - K_2) \sin \theta_p \cos \theta_p & K_1 \sin^2 \theta_p + K_2 \cos^2 \theta_p \end{bmatrix} \tag{4}$$

The inverse matrix of $\boldsymbol{K}$ in Eq. (2) can be given as:

$$\boldsymbol{K}^{-1} = \frac{1}{K_1 K_2} \begin{bmatrix} K_1 \sin^2 \theta_p + K_2 \cos^2 \theta_p & (K_2 - K_1) \sin \theta_p \cos \theta_p \\ (K_2 - K_1) \sin \theta_p \cos \theta_p & K_1 \cos^2 \theta_p + K_2 \sin^2 \theta_p \end{bmatrix} \tag{5}$$

The Forchheimer coefficient tensor $\boldsymbol{C}_{\boldsymbol{F}}$ can be given as:

$$\boldsymbol{C}_{\boldsymbol{F}} = \begin{bmatrix} \frac{F_1}{\sqrt{K_1}} \cos^2 \theta_p + \frac{F_2}{\sqrt{K_2}} \sin^2 \theta_p & \left(\frac{F_1}{\sqrt{K_1}} - \frac{F_2}{\sqrt{K_2}} \right) \sin \theta_p \cos \theta_p \\ \left(\frac{F_1}{\sqrt{K_1}} - \frac{F_2}{\sqrt{K_2}} \right) \sin \theta_p \cos \theta_p & \frac{F_2}{\sqrt{K_2}} \cos^2 \theta_p + \frac{F_1}{\sqrt{K_1}} \sin^2 \theta_p \end{bmatrix} \tag{6}$$

where F_1 and F_2 are the geometric function. The Ergun's equation can be employed to evaluate F's value, e.g. for the granular porous medium, F_1 can be expressed as:

$$F_1 = \frac{1.75}{\sqrt{150\varepsilon^3}} \tag{7}$$

For the anisotropic thermal conductivity of the solid matrix, the principal effective thermal conductivities of the solid matrix are κ_{em1} and κ_{em2}, respectively. The angle between κ_{em1} direction and x-direction is θ_t. Then the effective conductivity tensor $\boldsymbol{\kappa}_{em}$ can be given by the following matrix:

$$\boldsymbol{\kappa}_{em} = \begin{bmatrix} \kappa_{em1}\cos^2\theta_t + \kappa_{em2}\sin^2\theta_t & (\kappa_{em1}-\kappa_{em2})\sin\theta_t\cos\theta_t \\ (\kappa_{em1}-\kappa_{em2})\sin\theta_t\cos\theta_t & \kappa_{em1}\sin^2\theta_t + \kappa_{em2}\cos^2\theta_t \end{bmatrix} \tag{8}$$

The effective thermal conductivity κ_e determined by the thermal conductivities of each constituent and the microstructural characteristics such as porosity and pore diameter distribution can be estimated by the effective medium theory (EMT) [14]. However, a simplified equation is adopted in the present study, which yields the following formulation:

$$\begin{aligned} \kappa_{ef} &= \varepsilon\kappa_f \\ \kappa_{em} &= (1-\varepsilon)\kappa_m \end{aligned} \tag{9}$$

where the κ_f and κ_m are the thermal conductivity of the fluid and solid, respectively.

The convective flow and heat transfer can be characterized by several dimensionless parameters, which are given as follow:

$$\begin{aligned} &Ra = \frac{g\beta_T L^3\Delta T}{\nu_f\alpha_f}, Pr = \frac{\nu_f}{\alpha_f}, \quad Da = \frac{K_1}{L^2}, \\ &J = \frac{\nu_e}{\nu_f}, \lambda = \frac{\kappa_m}{\kappa_f}, \gamma = \frac{\kappa_{em1}}{\kappa_{ef}} \\ &\sigma = \frac{(\rho c_p)_m}{(\rho c_p)_f}, Hv = \frac{h_v L^2}{\kappa_f}, \\ &Ha_f = \frac{Q_f L^2}{\Delta T}, Ha_m = \frac{Q_m L^2}{\Delta T} \end{aligned} \tag{10}$$

where Ra is the Rayleigh number; Pr is the Prandtl number; Da is the Darcy number; J is the viscosity ratio of the effective viscosity to the fluid viscosity; γ is the ratio of the effective conductivity; λ is the thermal conductivity ratio of the solid matrix to the fluid; σ is the heat capacity ratio of the solid matrix to the fluid; Hv is the dimensionless volumetric heat transfer coefficient; Ha is the dimensionless volumetric heat generation rate; $\Delta T=T_h-T_c$ or QL/κ_f is the characteristic temperature difference. We also define three non-dimensional parameters to take into the anisotropic media consideration: the ratio of Forchheimer constants R_C, the ratio of permeability R_K and the ratio of thermal conductivity R_κ, which are given as:

$$R_C = \frac{F_2}{F_1}, R_K = \frac{K_2}{K_1}, R_\kappa = \frac{\kappa_{m2}}{\kappa_{m1}} \tag{11}$$

3. Multiple-Relaxation-Time Lattice Boltzmann Model

A MRT lattice Boltzmann model is then established to model the natural convective heat transfer in the hydrodynamically and thermally anisotropic porous medium under LTNE conditions at the REV scale. The proposed thermal LB model consists of three sets of distribution function, one for the flow field based on the generalized non-Darcy model, and the other two sets for the temperature fields of the fluid and solid matrix under the LNTE conditions, respectively. The flow field and the fluid temperature field couple with each other by the buoyancy source term, while the fluid temperature field and the solid temperature field couple with each other by the source term for the interfacial heat transfer between the solid and fluid phase.

The D2Q9 discrete velocity set is adopted to solve the velocity and temperature field in the present study, the corresponding nine discrete velocities are given as:

$$\boldsymbol{e}_\alpha = \begin{cases} c(0,0) & \alpha=0 \\ c\left(\cos\dfrac{(\alpha-1)\pi}{2}, \sin\dfrac{(\alpha-1)\pi}{2}\right) & \alpha=1,2,3,4 \\ \sqrt{2}c\left(\cos\dfrac{(2\alpha-9)\pi}{4}, \sin\dfrac{(2\alpha-9)\pi}{4}\right) & \alpha=5,6,7,8 \end{cases} \tag{12}$$

where α is the discrete velocity direction; and c is the lattice speed, defined as $c=\delta_x/\delta_t$ with δ_x and δ_t are the lattice spacing and time step, respectively. It should be noted that both δ_x and δ_t, as well as all the other variables in this study, are given to be dimensionless and $c=\delta_x/\delta_t=1$. The corresponding weighted coefficient w_α satisfies the following conditions:

$$\begin{aligned} &\sum_\alpha w_\alpha = 1, \quad \sum_\alpha w_\alpha \boldsymbol{e}_\alpha = 0, \\ &\sum_\alpha w_\alpha e_{\alpha,i} e_{\alpha,j} = c_s^2\delta_{ij}, \quad \sum_\alpha w_\alpha e_{\alpha,i} e_{\alpha,j} e_{\alpha,k} = 0, \\ &\sum_\alpha w_\alpha e_{\alpha,i} e_{\alpha,j} e_{\alpha,k} e_{\alpha,l} = \Delta_{ijkl} \end{aligned} \tag{13}$$

where δ_{ij} is the Kronecker delta with two indices i and j, $\Delta_{ijkl}=\delta_{ij}\delta_{kl}+\delta_{ik}\delta_{jl}+\delta_{il}\delta_{jk}$.

The lattice Boltzmann equation with the MRT collision scheme can be expressed as:

$$f_\alpha^k\left(\boldsymbol{x}+\boldsymbol{e}_\alpha\delta_t,\ t+\delta_t\right)= f_\alpha^k\left(\boldsymbol{x},\ t\right)-\left[\boldsymbol{M}^{-1}\boldsymbol{S}^k\left(\boldsymbol{m}^k-\boldsymbol{m}^{k,\,eq}\right)\left(\boldsymbol{x},\ t\right)\right]_\alpha +\delta_t\left(\boldsymbol{M}^{-1}\left(\mathbf{I}-\frac{\boldsymbol{S}^k}{2}\right)\boldsymbol{F}_m^k\left(\boldsymbol{x},\ t\right)\right)_\alpha \tag{14}$$

which can be decomposed into two steps, i.e., the collision process:

$$\bar{f}_\alpha^k\left(\boldsymbol{x},\ t\right)= f_\alpha^k\left(\boldsymbol{x},\ t\right)-\left[\boldsymbol{M}^{-1}\boldsymbol{S}\left(\boldsymbol{m}^k-\boldsymbol{m}^{k,\,eq}\right)\left(\boldsymbol{x},\ t\right)\right]_\alpha +\delta_t\left[\boldsymbol{M}^{-1}\left(\boldsymbol{I}-\frac{\boldsymbol{S}}{2}\right)\boldsymbol{F}_m^k\left(\boldsymbol{x},\ t\right)\right]_\alpha \tag{15}$$

and the streaming process:

$$f_\alpha^k\left(\boldsymbol{x}+\boldsymbol{e}_\alpha\delta_t,\ t+\delta_t\right)=\bar{f}_\alpha^k\left(\boldsymbol{x},\ t\right) \tag{16}$$

where f_α^k is the poststreaming distribution function; $\bar{f}_\alpha^k$ is the postcollision distribution function. The superscript "k" denotes the velocity field when $k = \boldsymbol{u}$ or the temperature field for the fluid phase when $k = T_f$ and solid matrix when $k = T_m$, respectively. $\boldsymbol{I}$ is the unit matrix; $\boldsymbol{M}$ is a 9×9 orthogonal transformation matrix, $\boldsymbol{m}^k=\boldsymbol{M}\boldsymbol{f}^k$ and $\boldsymbol{m}^{k,\,eq}=\boldsymbol{M}\boldsymbol{f}^{k,eq}$ are the vectors for the moments of the distribution function and its corresponding equilibrium moments vector, respectively. $\boldsymbol{S}^k=\boldsymbol{M}\boldsymbol{\Lambda}^k\boldsymbol{M}^{-1}$ is a non-negative 9×9 relaxation matrix in the moment space, which can be chosen as either a diagonal matrix or a non-diagonal matrix for a specific problem. $\boldsymbol{\Lambda}^k$ is the relaxation matrix in the discrete velocity space. $\boldsymbol{F}_m^k$ is the discrete force term in the moment space. For D2Q9 model, the transformation matrix $\boldsymbol{M}$ can be chosen as:

$$\boldsymbol{M}=\begin{bmatrix} 1 & 1 & 1 & 1 & 1 & 1 & 1 & 1 & 1\\ -4 & -1 & -1 & -1 & -1 & 2 & 2 & 2 & 2\\ 4 & -2 & -2 & -2 & -2 & 1 & 1 & 1 & 1\\ 0 & 1 & 0 & -1 & 0 & 1 & -1 & -1 & 1\\ 0 & -2 & 0 & 2 & 0 & 1 & -1 & -1 & 1\\ 0 & 0 & 1 & 0 & -1 & 1 & 1 & -1 & -1\\ 0 & 0 & -2 & 0 & 2 & 1 & 1 & -1 & -1\\ 0 & 1 & -1 & 1 & -1 & 0 & 0 & 0 & 0\\ 0 & 0 & 0 & 0 & 0 & 1 & -1 & 1 & -1 \end{bmatrix} \tag{17}$$

3.1 MRT-LB model for the flow field

For the velocity field (k=$\boldsymbol{u}$), the equilibrium moments vector $\boldsymbol{m}^{\boldsymbol{u},\,eq}$ can be given by:

$$\boldsymbol{m}^{\boldsymbol{u},\,eq}=\left(\rho_f,\ -2\rho_f+\frac{3\rho_0\boldsymbol{u}^2}{\varepsilon},\ \rho_f-\frac{3\rho_0\boldsymbol{u}^2}{\varepsilon},\ \rho_0u_x,\ -\rho_0u_x,\ \rho_0u_y,\ -\rho_0u_y,\ \frac{\rho_0\left(u_x^2-u_y^2\right)}{\varepsilon},\ \rho_0u_xu_y\right)^{\mathrm{T}} \tag{18}$$

It should be noted that an incompressible LB model with a modified equilibrium distribution function is adopted in the present work, the corresponding equilibrium distribution function in the discrete velocity field can be given as:

$$f_\alpha^{\boldsymbol{u},eq}= w_\alpha\left\{\rho_f+\rho_0\left[\frac{\boldsymbol{e}_\alpha\cdot\boldsymbol{u}}{c_s^2}+\frac{\left(\boldsymbol{e}_\alpha\cdot\boldsymbol{u}\right)^2}{2\varepsilon c_s^4}-\frac{\boldsymbol{u}^2}{2\varepsilon c_s^2}\right]\right\} \tag{19}$$

where the mean density ρ_0 is set to be 1.0; the lattice sound speed c_s is defined as $c_s=c/\sqrt{3}$ for the D2Q9 model. The corresponding relaxation matrix in the moment space $\boldsymbol{S}^{\boldsymbol{u}}$ can be chosen as a diagonal matrix:

$$\boldsymbol{S}^{\boldsymbol{u}}=\mathrm{diag}\left(s_c^{\boldsymbol{u}},s_e^{\boldsymbol{u}},s_\varepsilon^{\boldsymbol{u}},s_j^{\boldsymbol{u}},s_q^{\boldsymbol{u}},s_j^{\boldsymbol{u}},s_q^{\boldsymbol{u}},s_\nu^{\boldsymbol{u}},s_\nu^{\boldsymbol{u}}\right) \tag{20}$$

And these parameters can be chosen as:

$$s_0^u=s_3^u=s_5^u=1.0,\ s_1^u=s_2^u=1.4,\quad s_4^u=s_6^u=1.2,\ s_7^u=s_8^u=1/\tau_f \tag{21}$$

where

$$\nu_e=c_s^2\delta_t\left(\tau_f-0.5\right) \tag{22}$$

For avoiding error terms induced by the unsteady and non-uniform force, the discrete force term vector $\boldsymbol{F}_{\boldsymbol{m}}^{\boldsymbol{u}}$ can be given as:

$$\boldsymbol{F}_{\boldsymbol{m}}^{\boldsymbol{u}}=\left(0,\frac{6\rho_0\boldsymbol{u}\cdot\boldsymbol{F}_b}{\varepsilon},-\frac{6\rho_0\boldsymbol{u}\cdot\boldsymbol{F}_b}{\varepsilon},\rho_0F_{bx},-\rho_0F_{bx},\ \rho_0F_{by},-\rho_0F_{by},\frac{2\rho_0\left(u_xF_{bx}-u_yF_{by}\right)}{\varepsilon},\ \frac{2\rho_0\left(u_xF_{by}+u_yF_{bx}\right)}{\varepsilon}\right)^{\mathrm{T}} \tag{23}$$

where $\boldsymbol{F}_b$=($\boldsymbol{F}_{bx}$, $\boldsymbol{F}_{by}$) is the force term represented by Eq. (2).

With the distribution function evolving on the discrete lattices, the corresponding macro-quantities can be computed as:

$$\rho_f=\sum_\alpha f_\alpha^{\boldsymbol{u}},\ \rho_f\boldsymbol{u}=\sum_\alpha f_\alpha^{\boldsymbol{u}}\boldsymbol{e}_\alpha+\frac{\delta_t}{2}\rho_f\boldsymbol{F}_b,\ p=c_s^2\rho_f/\varepsilon \tag{24}$$

It should be noted that the force term $\boldsymbol{F}_b$ is the nonlinear function of the velocity $\boldsymbol{u}$, and with the help of Eq. (2), a nonlinear implicit form of the velocity $\boldsymbol{u}$

can be derived:

$$\rho_f\left(\boldsymbol{I}+\frac{\delta_t}{2}\varepsilon\nu_f\boldsymbol{K}^{-1}+\frac{\delta_t}{2}\varepsilon\boldsymbol{C_F}\left|\boldsymbol{u}\right|\right)\boldsymbol{u}=\sum_i f_\alpha^{\boldsymbol{u}}\boldsymbol{e}_\alpha+\frac{\delta_t}{2}\rho_f\varepsilon\boldsymbol{G} \tag{25}$$

It is difficult to obtain an explicit solution for this nonlinear implicit equation. To keep the merit of the high computational efficiency of the LBM, we replace the nonlinear term $\left|\boldsymbol{u}(t+\delta t)\right|\boldsymbol{u}(t+\delta t)$ with $\left|\boldsymbol{u}(t)\right|\boldsymbol{u}(t+\delta t)$ as suggested by Hu et al. [12]. Thus, an approximate explicit solution for the velocity can be obtained:

$$\boldsymbol{u}(t+\delta t)=\left(\boldsymbol{I}+\frac{\delta_t}{2}\varepsilon\nu_f\boldsymbol{K}^{-1}+\frac{\delta_t}{2}\varepsilon\boldsymbol{C_F}\left|\boldsymbol{u}(t)\right|\right)^{-1}\left(\frac{\sum_\alpha f_\alpha^{\boldsymbol{u}}\boldsymbol{e}_\alpha}{\rho_f}+\frac{\delta_t}{2}\varepsilon\boldsymbol{G}\right) \tag{26}$$

Through the Chapman-Enskog analysis, the proposed MRT-LB model for the velocity field can recover Eq. (1a) and Eq. (1b) in the incompressible limit where the Mach number is small enough.

3.2 MRT-LB model for the temperature fields

For the temperature field of the fluid phase and solid matrix phase, a two-temperature MRT-LB model is developed to solve the energy equations under LTNE conditions depicted by Eq. (1c) and Eq. (1d). Particularly, by constructing two newly equilibrium distribution functions, as well as choosing two special relaxation matrixes with some additional off-diagonal elements inspired by Huang et al. [14], the convection-diffusion equation for fluid phase and the diffusion equation for the solid matrix with anisotropic diffusion coefficient without the unwanted deviation term can be recovered exactly through the Chapman-Enskog analysis.

For the fluid temperature field ($k=T_f$) and the solid matrix temperature field ($k=T_m$), two newly equilibrium distribution functions are constructed to solve Eq. (1c) and Eq. (1d), which can be given as:

$$f_\alpha^{T_f,eq}=\begin{cases}\left(\varepsilon_{ref}-\varepsilon\right)T_f+w_\alpha\varepsilon_{ref}T_f, & \alpha=0\\ w_\alpha T_f\left(\varepsilon_{ref}+\left(2\boldsymbol{e}_\alpha\cdot\boldsymbol{u}\right)/c_s^2\right), & \alpha=1,2,3,4\\ w_\alpha T_f\left(\varepsilon_{ref}+\left(\boldsymbol{e}_\alpha\cdot\boldsymbol{u}\right)/2c_s^2\right), & \alpha=5,6,7,8\end{cases} \tag{27a}$$

$$f_\alpha^{T_m,eq}=\begin{cases}\left(\varepsilon_{ref}-\varepsilon\right)T_m+w_\alpha\left(1-\varepsilon_{ref}\right)T_m, & \alpha=0\\ w_\alpha\left(1-\varepsilon_{ref}\right)T_m, & \alpha=1,2,3,4,5,6,7,8\end{cases} \tag{27b}$$

The corresponding weighted coefficient w_α can be defined as w_0=5/9, $w_{1,2,3,4,5,6,7,8}$=1/18. It should be noted that the reference porosity ε_{ref} which keeps unvaried over the entire space is introduced into the equilibrium function. Benefit from this treatment, the present LB model can be used to tackle the problem with the variation of the porosity which cannot be correctly solved by many previous LB models. We will give the details in the next section. In the computation, ε_{ref} can be chosen as the harmonic mean of the overall porosity of the domain. The corresponding equilibrium moments function vector $\boldsymbol{m}^{k,eq}$ are given by:

$$\boldsymbol{m}^{T_f,eq}=\left(\varepsilon T_f,\ -2T_f\left(2\varepsilon-\varepsilon_{ref}\right),\ 2T_f\left(2\varepsilon-\varepsilon_{ref}\right),T_f\frac{u_x}{c},\ -T_f\frac{u_x}{c},\ T_f\frac{u_y}{c},\ -T_f\frac{u_y}{c},\ 0,0\right)^T \tag{28a}$$

$$\boldsymbol{m}^{T_m,eq}=\left(\left(1-\varepsilon\right)T_m,\ -2T_m\left(\varepsilon_{ref}-2\varepsilon+1\right),2T_m\left(\varepsilon_{ref}-2\varepsilon+1\right),\ 0,\ 0,\ 0,\ 0,\ 0,0\right)^T \tag{28b}$$

Followed by the inspiration of Huang and Wu [14], some additional off-diagonal elements are introduced into the relaxation matrix to account for the anisotropic heat transfer and eliminate the unwanted deviation term induced by the influence of the convection term on the diffusion term when the velocity vector varies with space or time.

The relaxation matrix for the fluid temperature field ($k=T_f$) can be given as:

$$S^{T_f}=\begin{bmatrix} s_0^{T_f}, & 0, & 0, & 0, & 0, & 0, & 0, & 0, & 0 \\ 0, & s_1^{T_f}, & 0, & 0, & 0, & 0, & 0, & 0, & 0 \\ 0, & 0, & s_2^{T_f}, & 0, & 0, & 0, & 0, & 0, & 0 \\ 0, & 0, & 0, & s_{xx}^{T_f}, & \left(\frac{s_{xx}^{T_f}}{2}-1\right)s_4^{T_f}, & s_{xy}^{T_f}, & \frac{s_{xy}^{T_f}s_6^{T_f}}{2}, & 0, & 0 \\ 0, & 0, & 0, & 0, & s_4^{T_f}, & 0, & 0, & 0, & 0 \\ 0, & 0, & 0, & s_{xy}^{T_f}, & \frac{s_{xy}^{T_f}s_4^{T_f}}{2}, & s_{yy}^{T_f}, & \left(\frac{s_{yy}^{T_f}}{2}-1\right)s_6^{T_f}, & 0, & 0 \\ 0, & 0, & 0, & 0, & 0, & 0, & s_6^{T_f}, & 0, & 0 \\ 0, & 0, & 0, & 0, & 0, & 0, & 0, & s_7^{T_f}, & 0 \\ 0, & 0, & 0, & 0, & 0, & 0, & 0, & 0, & s_8^{T_f} \end{bmatrix} \tag{29a}$$

and the corresponding relaxation matrix for the solid matrix temperature field ($k=T_m$) can be expressed as:

$$S^{T_m}=\begin{bmatrix} s_0^{T_m}, & 0, & 0, & 0, & 0, & 0, & 0, & 0, & 0 \\ 0, & s_1^{T_m}, & 0, & 0, & 0, & 0, & 0, & 0, & 0 \\ 0, & 0, & s_2^{T_m}, & 0, & 0, & 0, & 0, & 0, & 0 \\ 0, & 0, & 0, & s_{xx}^{T_m}, & 0, & s_{xy}^{T_m}, & 0, & 0, & 0 \\ 0, & 0, & 0, & 0, & s_4^{T_m}, & 0, & 0, & 0, & 0 \\ 0, & 0, & 0, & s_{xy}^{T_m}, & 0, & s_{yy}^{T_m}, & 0, & 0, & 0 \\ 0, & 0, & 0, & 0, & 0, & 0, & s_6^{T_m}, & 0, & 0 \\ 0, & 0, & 0, & 0, & 0, & 0, & 0, & s_7^{T_m}, & 0 \\ 0, & 0, & 0, & 0, & 0, & 0, & 0, & 0, & s_8^{T_m} \end{bmatrix} \tag{29b}$$

It should be noted that the matrix $\boldsymbol{A}^k$ for $\boldsymbol{A}^{T_f}=\begin{pmatrix} s_{xx}^{T_f} & s_{xy}^{T_f} \\ s_{xy}^{T_f} & s_{yy}^{T_f} \end{pmatrix}$ and $\boldsymbol{A}^{T_m}=\begin{pmatrix} s_{xx}^{T_m} & s_{xy}^{T_m} \\ s_{xy}^{T_m} & s_{yy}^{T_m} \end{pmatrix}$ are introduced to account for the anisotropic diffusion, while the additional off-diagonal elements matrix $\boldsymbol{B}^{T_f}=\begin{pmatrix} \left(\frac{s_{xx}^{T_f}}{2}-1\right)s_4^{T_f} & \frac{s_{xy}^{T_f}s_6^{T_f}}{2} \\ \frac{s_{xy}^{T_f}s_4^{T_f}}{2} & \left(\frac{s_{yy}^{T_f}}{2}-1\right)s_6^{T_f} \end{pmatrix}$ is introduced to eliminate the unwanted deviation term when the fluid velocity vector varies with space or time. The corresponding discrete heat source term vector $\boldsymbol{F}_m^{T_f}$ and $\boldsymbol{F}_m^{T_m}$ can be given as:

$$F_m^{T_f}=q^{T_f}\left(1,-2,1,0,0,0,0,0,0\right)^T \tag{30a}$$

$$F_m^{T_m}=q^{T_m}\left(1,-2,1,0,0,0,0,0,0\right)^T \tag{30b}$$

where the effective heat source term can be expressed as:

$$q^{T_f}=\frac{h\left(T_m-T_f\right)+\varepsilon Q_f}{\left(\rho c_p\right)_f} \tag{31a}$$

$$q^{T_m}=\frac{h\left(T_f-T_m\right)+\left(1-\varepsilon\right)Q_m}{\left(\rho c_p\right)_m} \tag{31b}$$

The corresponding macro-quantities T_f and T_m then can be computed as:

$$\varepsilon T_f=\sum\nolimits_\alpha f_\alpha^{T_f}+\frac{\delta t}{2}q^{T_f}=m_0^{T_f}+\frac{\delta t}{2}q^{T_f} \tag{32a}$$

$$\left(1-\varepsilon\right)T_m=\sum\nolimits_\alpha f_\alpha^{T_m}+\frac{\delta t}{2}q^{T_m}=m_0^{T_m}+\frac{\delta t}{2}q^{T_m} \tag{32b}$$

Since the effective heat source terms also contain the priori unknowns T_f and T_m, Eq. (32a) and Eq. (32b) are implicit linear equations. The corresponding explicit solutions are given as:

$$T_f=\frac{\left((1-\varepsilon)+\dfrac{\delta_t h_v}{2\left(\rho c_p\right)_m}\right)\left(\sum_{\alpha=0}^{\alpha=8} f_\alpha^{T_f}+\dfrac{\delta_t \varepsilon Q_f}{2\left(\rho c_p\right)_f}\right)+\dfrac{\delta_t h_v}{2\left(\rho c_p\right)_f}\left(\sum_{\alpha=0}^{\alpha=8} f_\alpha^{T_m}+\dfrac{\delta_t(1-\varepsilon)Q_m}{2\left(\rho c_p\right)_m}\right)}{\left[(1-\varepsilon)+\dfrac{\delta_t h_v}{2\left(\rho c_p\right)_m}\right]\left[\varepsilon+\dfrac{\delta_t h_v}{2\left(\rho c_p\right)_f}\right]-\dfrac{\delta_t h_v}{2\left(\rho c_p\right)_f}\dfrac{\delta_t h_v}{2\left(\rho c_p\right)_m}} \tag{33a}$$

$$T_m=\frac{\dfrac{\delta_t h_v}{2\left(\rho c_p\right)_m}\left(\sum_{\alpha=0}^{\alpha=8} f_\alpha^{T_f}+\dfrac{\delta_t \varepsilon Q_f}{2\left(\rho c_p\right)_f}\right)+\left[\varepsilon+\dfrac{\delta_t h_v}{2\left(\rho c_p\right)_f}\right]\left(\sum_{\alpha=0}^{\alpha=8} f_\alpha^{T_m}+\dfrac{\delta_t(1-\varepsilon)Q_m}{2\left(\rho c_p\right)_m}\right)}{\left[(1-\varepsilon)+\dfrac{\delta_t h_v}{2\left(\rho c_p\right)_m}\right]\left[\varepsilon+\dfrac{\delta_t h_v}{2\left(\rho c_p\right)_f}\right]-\dfrac{\delta_t h_v}{2\left(\rho c_p\right)_f}\dfrac{\delta_t h_v}{2\left(\rho c_p\right)_m}} \tag{33b}$$

3.3 Chapman-Enskog analysis

Then, the Chapman-Enskog analysis is performed to recover the energy equations for the temperature fields under LTNE. By introducing a small parameter ζ, the moments of the distribution function and the derivatives of space and time can be expanded as:

$$\begin{aligned}&\boldsymbol{m}^k=\boldsymbol{m}^{k,(0)}+\zeta^1\boldsymbol{m}^{k,(1)}+\zeta^2\boldsymbol{m}^{k,(2)}+\zeta^3\boldsymbol{m}^{k,(3)}+\cdots\\&\partial_t=\zeta\partial_{t1}+\zeta^2\partial_{t2},\quad \partial_x=\zeta\partial_{x1},\quad \partial_y=\zeta\partial_{y1}\\&\boldsymbol{F}_m^k(\boldsymbol{x},\,t)=\zeta\boldsymbol{F}_m^{k,(1)}(\boldsymbol{x},\,t)\end{aligned} \tag{34}$$

where $t1$ and $t2$ are the convective time scale and diffusion time scale, respectively.

Taking the Taylor series expansion for Eq. (14) and rewriting it, we can get:

$$\begin{aligned}&\hat{\boldsymbol{D}}\boldsymbol{m}^k+\frac{\delta_t}{2}\hat{\boldsymbol{D}}^2\boldsymbol{m}^k+O\left(\delta_t^2\right)=\\&\quad-\frac{\boldsymbol{S}^k}{\delta}\left(\boldsymbol{m}^k-\boldsymbol{m}^{k,eq}\right)+\left(\boldsymbol{I}-\frac{\boldsymbol{S}^k}{2}\right)\boldsymbol{F}_m^k\end{aligned} \tag{35}$$

where $\hat{\boldsymbol{D}}=\boldsymbol{I}\partial_t+\boldsymbol{E}\cdot\nabla=(\zeta\partial_{t1}+\zeta^2\partial_{t2})\boldsymbol{I}+\zeta\boldsymbol{E}\cdot\nabla_1=\zeta\hat{\boldsymbol{D}}_1+\zeta^2\partial_{t2}\boldsymbol{I}$, $\hat{\boldsymbol{D}}_1=\boldsymbol{I}\partial_{t1}+\boldsymbol{E}\cdot\nabla_1$, in which $\boldsymbol{E}$=($\boldsymbol{E_x}$, $\boldsymbol{E_y}$), and $\boldsymbol{E_x}=\boldsymbol{M}\left[diag\left(e_{0x},e_{1x},e_{2x},e_{3x},e_{4x},e_{5x},e_{6x},e_{7x},e_{8x}\right)\right]\boldsymbol{M}^{-1}$, $\boldsymbol{E}_y=\boldsymbol{M}\left[diag\left(e_{0y},e_{1y},e_{2y},e_{3y},e_{4y},e_{5y},e_{6y},e_{7y},e_{8y}\right)\right]\boldsymbol{M}^{-1}$.

Substituting Eq. (34) into Eq. (35), the following equations in the consecutive orders of the small expansion parameter ζ can be obtained:

$$\zeta^{(0)}:\ \boldsymbol{m}^{k,(0)}=\boldsymbol{m}^{k,eq} \tag{36a}$$

$$\zeta^{(1)}:\ \hat{\boldsymbol{D}}_1\boldsymbol{m}^{k,(0)}=-\frac{\boldsymbol{S}^k}{\delta_t}\boldsymbol{m}^{k,(1)}+\left(\boldsymbol{I}-\frac{\boldsymbol{S}^k}{2}\right)\boldsymbol{F}_m^{k,(1)} \tag{36b}$$

$$\begin{aligned}&\zeta^{(2)}:\ \partial_{t2}\boldsymbol{m}^{k,(0)}+\hat{\boldsymbol{D}}_1\left(\boldsymbol{I}-\frac{\boldsymbol{S}^k}{2}\right)\left[\boldsymbol{m}^{k,(1)}+\frac{\delta_t\boldsymbol{F}_m^{k,(1)}}{2}\right]\\&=-\frac{\boldsymbol{S}^k}{\delta_t}\boldsymbol{m}^{k,(2)}\end{aligned} \tag{36c}$$

Rewriting it, we can get:

$$\zeta^{(0)}:\ \boldsymbol{m}^{k,(0)}=\boldsymbol{m}^{k,eq} \tag{37a}$$

$$\begin{aligned}&\zeta^{(1)}:\left(\boldsymbol{I}\partial_{t1}+\boldsymbol{E}_x\cdot\partial_{x1}+\boldsymbol{E}_y\cdot\partial_{y1}\right)\boldsymbol{m}^{k,(0)}-\boldsymbol{F}_m^{k,(1)}\\&=-\frac{\boldsymbol{S}^k}{\delta_t}\left(\boldsymbol{m}^{k,(1)}+\frac{\delta_t}{2}\boldsymbol{F}_m^{k,(1)}\right)\end{aligned} \tag{37b}$$

$$\begin{aligned}&\zeta^{(2)}:\ \partial_{t2}\boldsymbol{m}^{k,(0)}+\left(\boldsymbol{I}\partial_{t1}+\boldsymbol{E}_x\cdot\partial_{x1}+\boldsymbol{E}_y\cdot\partial_{y1}\right)\\&\left(\boldsymbol{I}-\frac{\boldsymbol{S}^k}{2}\right)\left(\boldsymbol{m}^{k,(1)}+\frac{\delta_t}{2}\boldsymbol{F}_m^{k,(1)}\right)=-\frac{\boldsymbol{S}^k}{\delta_t}\boldsymbol{m}^{k,(2)}\end{aligned} \tag{37c}$$

With the help of Eq. (34), Eq. (32a) and Eq. (40) can lead to the following relationships:

$$\zeta^{(0)}:m_0^{k,(0)}=m_0^{k,eq} \tag{38a}$$

$$\zeta^{(1)}:\ m_0^{k,(1)}+\frac{\delta_t F_{m0}^{k,(1)}}{2}=0 \tag{38b}$$

$$\zeta^{(n)}:\ m_0^{k,(n)}=0,\ n\geq 2 \tag{38c}$$

The equations for the conserved moment, m_0^k, in Eq. (37a) can be written as:

$$\zeta^{(0)}:m_0^{k,(0)}=m_0^{k,eq} \tag{39a}$$

$$\begin{aligned}&\zeta^{(1)}:\ \partial_{x1}m_3^{k,(0)}+\partial_{y1}m_5^{k,(0)}+\partial_{t1}m_0^{k,(0)}\\&=F_{m0}^{k,(1)}-\frac{s_0^k}{\delta_t}\left(m_0^{k,(1)}+\delta_t F_{m0}^{k,(1)}/2\right)=F_{m0}^{k,(1)}\end{aligned} \tag{39b}$$

$$\begin{aligned}&\zeta^{(2)}:\ \partial_{t2}m_0^{k,(1)}+\partial_{t1}\left[\left(m_0^{k,(1)}+\frac{\delta_t F_{m0}^{k,(1)}}{2}\right)\left(1-\frac{s_0^k}{2}\right)\right]\\&+\nabla_1\cdot\left(\boldsymbol{I}-\frac{\boldsymbol{A}^k}{2}\right)\\&\left(\begin{array}{c}\left(m_3^{k,(1)}+\dfrac{\delta_t F_{m3}^{(1)}}{2}\right)+\dfrac{s_4^k}{2}\left(m_4^{k,(1)}+\dfrac{\delta_t F_{m4}^{k,(1)}}{2}\right)\\\left(m_5^{k,(1)}+\dfrac{\delta_t F_{m5}^{(1)}}{2}\right)+\dfrac{s_6^k}{2}\left(m_6^{k,(1)}+\dfrac{\delta_t F_{m6}^{k,(1)}}{2}\right)\end{array}\right)\\&=-\frac{s_0^k}{\delta t}m_0^{k,(2)}\end{aligned} \tag{39c}$$

With the help of Eq. (38), Eq. (39c) can be rewritten as:

$$\zeta^{(2)}:\ \partial_{t2}m_0^{k,(0)}+\nabla_1\cdot\left(\boldsymbol{I}-\frac{\boldsymbol{A}^k}{2}\right)\begin{pmatrix}\left(m_3^{k,(1)}+\dfrac{\delta_t F_{m3}^{(1)}}{2}\right)+\dfrac{s_4^k}{2}\left(m_4^{k,(1)}+\dfrac{\delta_t F_{m4}^{k,(1)}}{2}\right)\\ \left(m_5^{k,(1)}+\dfrac{\delta_t F_{m5}^{(1)}}{2}\right)+\dfrac{s_6^k}{2}\left(m_6^{k,(1)}+\dfrac{\delta_t F_{m6}^{k,(1)}}{2}\right)\end{pmatrix}=0 \tag{39d}$$

To further simplify Eq. (39d), by adding the fifth equation to the fourth equation of Eq. (37b), as well as adding the seventh equation to the sixth equation, and then combining the two resulting equations, we can get:

$$\begin{aligned}&\begin{pmatrix}\left(m_3^{k,(1)}+\delta_t\dfrac{F_{m3}^{k,(1)}}{2}\right)+\dfrac{s_4^k}{2}\left(m_4^{k,(1)}+\delta_t\dfrac{F_{m4}^{k,(1)}}{2}\right)\\ \left(m_5^{k,(1)}+\delta_t\dfrac{F_{m5}^{k,(1)}}{2}\right)+\dfrac{s_6^k}{2}\left(m_6^{k,(1)}+\delta_t\dfrac{F_{m6}^{k,(1)}}{2}\right)\end{pmatrix}=\\ &-\frac{\delta_t}{\boldsymbol{A}^k}\begin{pmatrix}\partial_{x1}\left(\dfrac{2m_0^{k,(0)}}{3}+\dfrac{m_1^{k,(0)}}{2}+\dfrac{m_2^{k,(0)}}{3}-\dfrac{m_7^{k,(0)}}{2}\right)+\partial_{y1}\left(2m_8^{k,(0)}\right)+\partial_{t1}\left(m_3^{k,(0)}+m_4^{k,(0)}\right)-\left(F_{m3}^{k,(1)}+F_{m4}^{k,(1)}\right)\\ \partial_{x1}\left(2m_8^{k,(0)}\right)+\partial_{y1}\left(\dfrac{2m_0^{k,(0)}}{3}+\dfrac{m_1^{k,(0)}}{2}+\dfrac{m_2^{k,(0)}}{3}+\dfrac{m_7^{k,(0)}}{2}\right)+\partial_{t1}\left(m_5^{k,(0)}+m_6^{k,(0)}\right)-\left(F_{m5}^{k,(1)}+F_{m6}^{k,(1)}\right)\end{pmatrix}\end{aligned} \tag{40}$$

Utilizing Eqs. (28) and (30), Eq. (40) can be simplified as:

$$\begin{pmatrix}\left(m^{k,(1)}+\delta_t\dfrac{F_{m3}^{k,(1)}}{2}\right)+\dfrac{s_4^k}{2}\left(m_4^{k,(1)}+\delta_t\dfrac{F_{m4}^{k,(1)}}{2}\right)\\ \left(m_5^{k,(1)}+\delta_t\dfrac{F_{m5}^{k,(1)}}{2}\right)+\dfrac{s_6^k}{2}\left(m_6^{k,(1)}+\delta_t\dfrac{F_{m6}^{k,(1)}}{2}\right)\end{pmatrix}=-\frac{\delta_t}{\boldsymbol{A}^k}\nabla_1\left(\frac{2m_0^{k,(0)}}{3}+\frac{m_1^{k,(0)}}{2}+\frac{m_2^{k,(0)}}{3}\right) \tag{41}$$

Thus, Eq. (39) can be rewritten as:

$$\zeta^{(1)}:\ \partial_{x1}m_3^{k,(0)}+\partial_{y1}m_5^{k,(0)}+\partial_{t1}m_0^{k,(0)}=q^{k,(1)} \tag{42a}$$

$$\zeta^{(2)}:\ \partial_{t2}m_0^{k,(0)}=\nabla_1\cdot\left[\left(\boldsymbol{I}-\frac{\boldsymbol{A}^k}{2}\right)\frac{\delta_t}{\boldsymbol{A}^k}\nabla_1\left(\frac{2m_0^{k,(0)}}{3}+\frac{m_1^{k,(0)}}{2}+\frac{m_2^{k,(0)}}{3}\right)\right] \tag{42b}$$

With the help of Eqs. (28), (30) and (38), the macroscopic equations in the $t1$ and $t2$ time scales for the fluid temperature field ($k=T_f$) can be obtained as:

$$\zeta^{(1)}:\ \partial_{t1}\varepsilon T_f+\partial_{x1}T_f u_x+\partial_{y1}T_f u_y=q^{T_f,(1)} \tag{43a}$$

$$\zeta^{(2)}:\ \partial_{t2}\varepsilon T_f=\nabla_1\cdot\left[\delta_t\left(\frac{1}{\boldsymbol{A}^{T_f}}-\frac{\boldsymbol{I}}{2}\right)\nabla_1\left(\frac{\varepsilon_{ref}T_f}{3}\right)\right] \tag{43b}$$

It's should be noted that the reference porosity ε_{ref} keeps unvaried over the entire space. Therefore, Eq. (43b) can be further modified as:

$$\zeta^{(2)}:\ \partial_{t2}\varepsilon T_f=\nabla_1\cdot\left[\frac{\delta_t\varepsilon_{ref}}{3}\left(\frac{1}{\boldsymbol{A}^{T_f}}-\frac{\boldsymbol{I}}{2}\right)\nabla_1 T_f\right] \tag{43c}$$

Combining the equations for the time scale t_1 and t_2, i.e., Eqs. (43a) and (43c), we recover the equation as:

$$\frac{\partial\varepsilon T_f}{\partial t}+\nabla\cdot\left(T_f\boldsymbol{u}\right)=\nabla\cdot\left[\frac{\delta_t\varepsilon_{ref}}{3}\left(\frac{1}{\boldsymbol{A}^{T_f}}-\frac{\boldsymbol{I}}{2}\right)\nabla T_f\right]+q^{T_f} \tag{44}$$

Therefore, the macroscopic energy equation for the fulid (Eq. (1c)) can be exactly recovered by setting:

$$\boldsymbol{\Gamma}^{T_f}=\frac{\boldsymbol{\kappa}_{ef}}{\left(\rho c_p\right)_f}=\frac{\delta_t\varepsilon_{ref}}{3}\left(\frac{1}{\boldsymbol{A}^{T_f}}-\frac{\boldsymbol{I}}{2}\right) \tag{45}$$

Similarly, the macroscopic equations in the $t1$ and $t2$ time scales for the solid matrix temperature field ($k=T_m$) can be obtained as:

$$\zeta^{(1)}:\ \partial_{t1}\left[\left(1-\varepsilon\right)T_m\right]=q^{T_m,(1)} \tag{46a}$$

$$\zeta^{(2)}:\ \partial_{t2}\left[\left(1-\varepsilon\right)T_m\right]=\nabla_1\cdot\left[\frac{1-\varepsilon_{ref}}{3}\delta_t\left(\frac{1}{\boldsymbol{A}^{T_m}}-\frac{\boldsymbol{I}}{2}\right)\nabla_1 T_m\right] \tag{46b}$$

The corresponding macroscopic equation can be obtained:

$$\frac{\partial\left(1-\varepsilon\right)T_m}{\partial t}=\nabla\cdot\left[\frac{1-\varepsilon_{ref}}{3}\delta_t\left(\frac{1}{\boldsymbol{A}^{T_m}}-\frac{\boldsymbol{I}}{2}\right)\nabla T_m\right]+q^{T_m} \tag{47}$$

The thermal diffusion coefficient matrix of the anisotropic solid matrix $\boldsymbol{\Gamma}^{T_m}$ can be given as:

$$\boldsymbol{\Gamma}^{T_m}=\frac{\boldsymbol{\kappa}_{em}}{\left(\rho c_p\right)_m}=\frac{1-\varepsilon_{ref}}{3}\delta_t\left(\frac{1}{\boldsymbol{A}^{T_m}}-\frac{\boldsymbol{I}}{2}\right) \tag{48}$$

Thus, the energy equation for the fluid and solid matrix under LTNE can be recovered exactly as:

$$\frac{\partial \varepsilon T_f}{\partial t}+\nabla\cdot\left(\boldsymbol{u}T_f\right)=\nabla\cdot\left(\boldsymbol{\Gamma}^{T_f}\nabla T_f\right)+\frac{h\left(T_m-T_f\right)+\varepsilon Q_f}{\left(\rho c_p\right)_f} \tag{49a}$$

$$\frac{\partial \left(1-\varepsilon\right)T_m}{\partial t}=\nabla\cdot\left(\boldsymbol{\Gamma}^{T_m}\nabla T\right)_m+\frac{h\left(T_f-T_m\right)+\left(1-\varepsilon\right)Q_m}{\left(\rho c_p\right)_m} \tag{49b}$$

Through the Chapman-Enskog analysis, the proposed MRT-LB model for the temperature fields can exactly recover Eq. (1c) and Eq. (1d) of no deviation terms without any additional assumptions. Additionally, in the present study, the fluid is assumed to be thermally isotropic, thus:

$$\boldsymbol{\Gamma}^{T_f}=\frac{\kappa_{ef}}{\left(\rho c_p\right)_f}\boldsymbol{I} \tag{50}$$

And the parameters for the relaxation matrix can be chosen as:

$$s_0^{T_f}=1.0,\ s_1^{T_f}=s_2^{T_f}=1.1,\ s_3^{T_f}=s_4^{T_f}=\frac{1}{s_{xx}^{T_f}},\ s_5^{T_f}=s_6^{T_f}=\frac{1}{s_{yy}^{T_f}},\ s_7^{T_f}=s_8^{T_f}=1.2\ \text{ and }\ s_{xx}^{T_f}=s_{yy}^{T_f} \tag{51a}$$

$$s_0^{T_m}=1.0,\ s_1^{T_m}=s_2^{T_m}=1.1,\ s_3^{T_m}=s_4^{T_m}=\frac{1}{s_{xx}^{T_m}},\ s_5^{T_m}=s_6^{T_m}=\frac{1}{s_{yy}^{T_m}},\ s_7^{T_m}=s_8^{T_m}=1.2 \tag{51b}$$

4. Numerical Results and Discussion

To evaluate the applicability of the proposed lattice Boltzmann model for the natural convection in anisotropic porous media under LTNE condition, numerical investigation of a natural convection problem in porous media is carried out. The simulated results are compared with the results reported in the literatures. Finally, the application of the proposed model considers the problem of natural convection in a hydrodynamically and thermally anisotropic porous medium under LTNE. In all cases, the non-equilibrium extrapolation schemes are applied to implement both the velocity and the thermal boundary condition [15, 16].

4.1 Natural convection in a heat generating isotropic porous medium

In the first case, the steady natural convection in an isotropic porous medium with internal heat generating solid matrix is investigated by the present LB model. As shown in Fig. 1, a square cavity with isothermally cooled walls is filled with a fluid-saturated porous medium which generates heat in solid matrix at a uniform rate Q_m. The four walls which are subjected to the no-slip velocity boundary conditions are cooled at a fixed temperature T_c. The characteristic temperature difference is given as $\Delta T=Q_fL/\kappa_f$. The dimensionless parameters characterizing this problem are given as follows: $Ra=10^7$, $Pr=7.0$, $Da=0.01$, $J=1.0$, $\gamma=1.0$, $Ha_f=0.0$, $Ha_m=1.0$. The other parameters are set as: $F_1=0.5648$, $R_C=1$, $R_K=1$, $R_\kappa=1$. Two cases with different dimensionless volumetric heat transfer coefficient H_v are simulated, which are set $H_v=1.0$ and 50.0, respectively.

The temperature profiles results at vertical mid-plane for different H_v by the present LB model are plotted in Fig. 2. It can be found that, for a very small interfacial heat transfer coefficient H_v (i.e. $H_v=1$), the temperature of the solid matrix is much higher than the temperature of the fluid phase, resulting from the very weak heat transfer between the solid matrix and fluid. Thus, the temperature difference between the phases is very large, indicating that the non-equilibrium effect is very strong when the interfacial heat transfer coefficient H_v is very small. With the increase of H_v, the temperature of the fluid increases, while the temperature of the solid matrix, as well as the temperature difference between the phases decrease, due to the enhancement of the heat transfer between the two phases. Therefore, the non-equilibrium effect will decrease with the interfacial heat transfer between the solid and fluid phase. When the H_v is large enough (i.e. $H_v=1000$), the local thermal equilibrium condition between the fluid and solid have been almost achieved. Additionally, the temperature profiles by the present LB model have been compared with the results reported in Ref. [2]. It can be observed that very good agreement can be achieved.

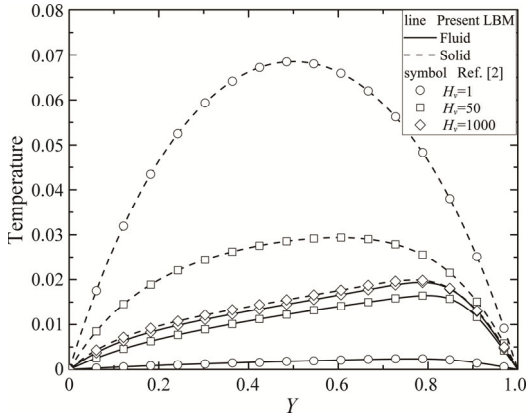

Fig. 2 The temperature profiles at vertical mid-plane for different H_v for $Ra=10^7$, $Pr=7.0$, $Da=0.01$, $J=1.0$, $\gamma=1.0$, $Ha_f=0.0$, $Ha_m=1.0$

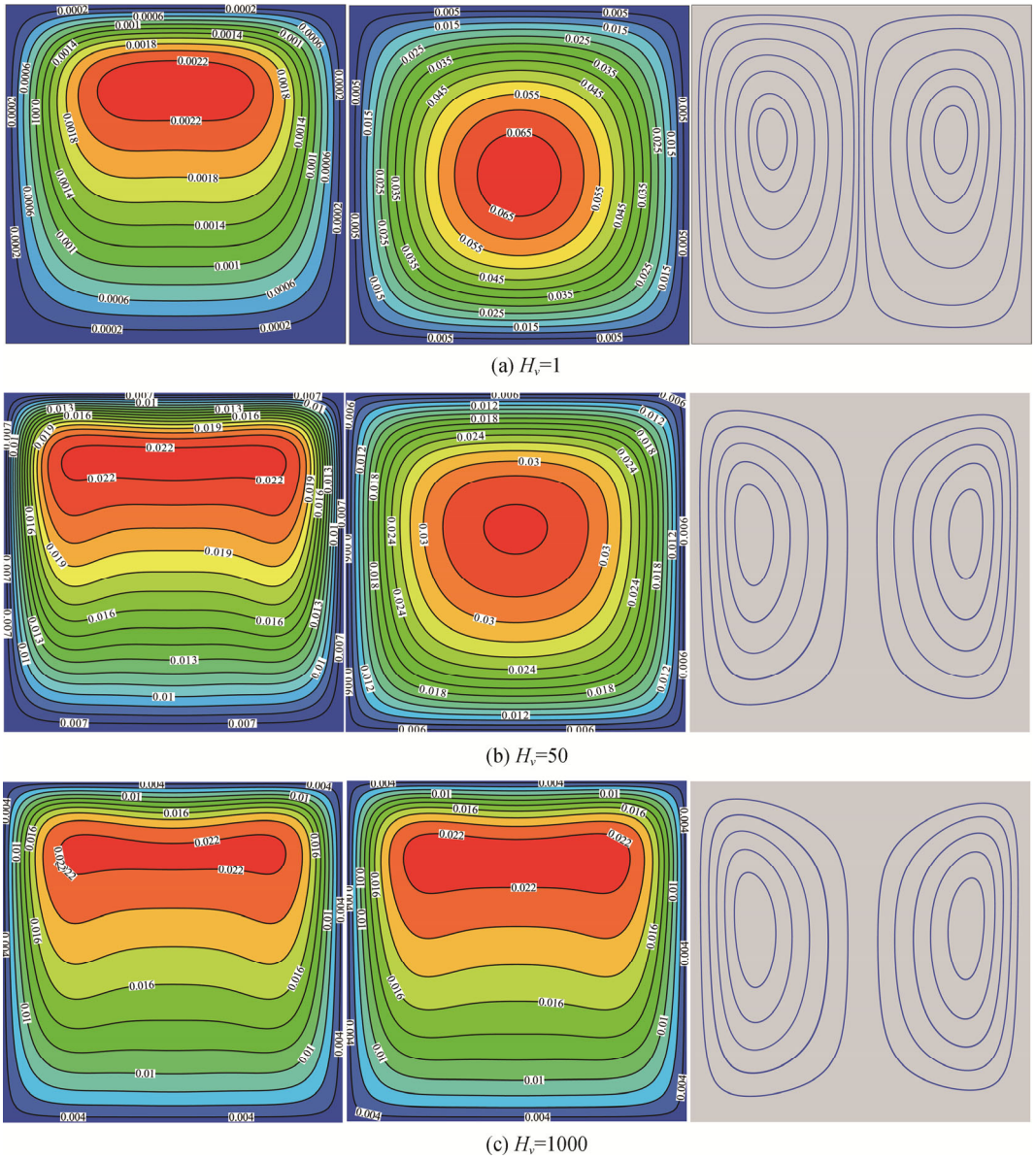

(a) H_v=1

(b) H_v=50

(c) H_v=1000

Fig. 3 The streamlines (right) and temperature distribution of fluid (left) and solid matrix (middle) for different interfacial heat transfer coefficient H_v

Fig. 3 shows the streamlines and temperature distribution of fluid and solid matrix for different interfacial heat transfer coefficient H_v. It can be observed that isotherms patterns of the fluid and solid matrix are evidently different for different parameters. And the temperature distribution for the fluid are different from that of the solid. The less the H_v is, the more evidently the difference between the solid temperature and fluid temperature is. It is observed that the flow consists of two eddies consisting of clockwise (right) and anti-clockwise (left) circulating vortices. It is also seen that the two circulating vortices are symmetrical with respect to the horizontal central plane of the cavity.

4.2 Natural convection in a heat generating anisotropic porous media

In the above test, the porous media is isotropic in thermal conductivity and permeability. To investigate the proposed LB model for the anisotropic porous media, the anisotropic effects of thermal conductivity and permeability are taken into account in this test. The dimensionless parameters characterizing this problem are given as follows: Ra=10^7, Pr=7.0, Da_1=0.01, J=1.0, γ=0.001, H_v =1.0, Ha_f=0.0, Ha_m=1.0, F_1=0.5648, R_C=1. The porous media is assumed to be thermally and hydrodynamically anisotropic. The interfacial heat transfer coefficients between the fluid and solid phase are

fixed to be H_v =1.0 for all cases. In this study, the permeability K_1 and thermal conductivity κ_1 are assumed to be constant; the permeability K_2 and thermal conductivity κ_2 are varied with permeability ratio R_K and thermal conductivity ratio R_κ. We investigate the influence of parameters such as R_K, R_κ and the inclination of principal axes (θ_p) by analysing in terms of streamlines, isotherms of the fluid and solid. We also investigate the influence of the ratio of vertical thermal conductivity to horizontal thermal conductivity for the solid matrix.

The influence of the hydrodynamical anisotropy is shown in Fig. 4 for θ_p=π/2 with the ratio of permeability R_K variation (Fig. 4(a)–(b)), as well as for R_K =0.01 with the inclination of principal axes (θ_p) variation (Fig. 4(b)–(c)). It is observed that the temperature distributions for solid matrix almost keep unvaried when interfacial heat transfer coefficient keeps constant regardless of the permeability of the flow field. This is because heat conduction is the dominating heat transfer mechanism for the solid. As shown from Fig. 4(a) and 4(b), the increase in R_K progressively strengths the natural convection due to increase in permeability in the direction of K_2. Additionally, the increase in permeability causes decrease in obstruction for the flow field and that promotes the flow and convective heat transfer transport, so the fluid temperature in Fig. 4(b) is higher than that of Fig. 4(a). With the increase in R_K, the maximum temperature for the fluid will decrease because of the fact that decrease in permeability will weaken the convection and thus weaken the internal heat transport. As shown in Fig. 4(c),

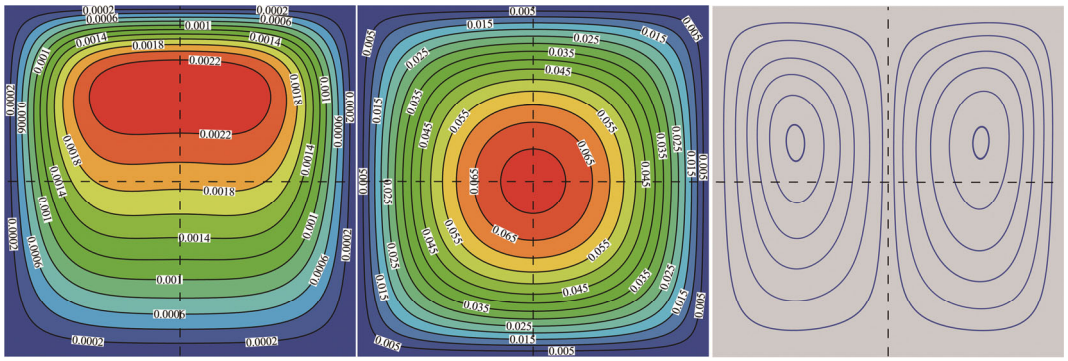

(a) θ_p=π/2, R_K=100

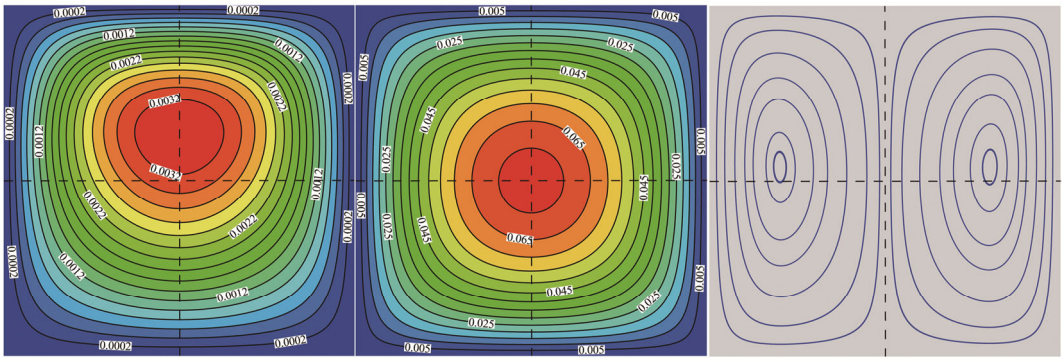

(b) θ_p=π/2, R_K=0.01

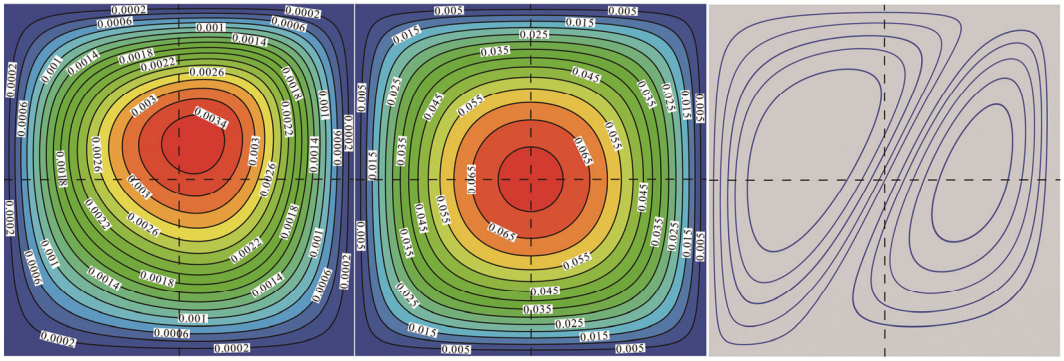

(c) θ_p=π/4, R_K=0.01

Fig. 4 The influence of the hydrodynamical anisotropy: the streamlines (right) and temperature distribution of fluid (left) and solid matrix (middle) for θ_p and R_K

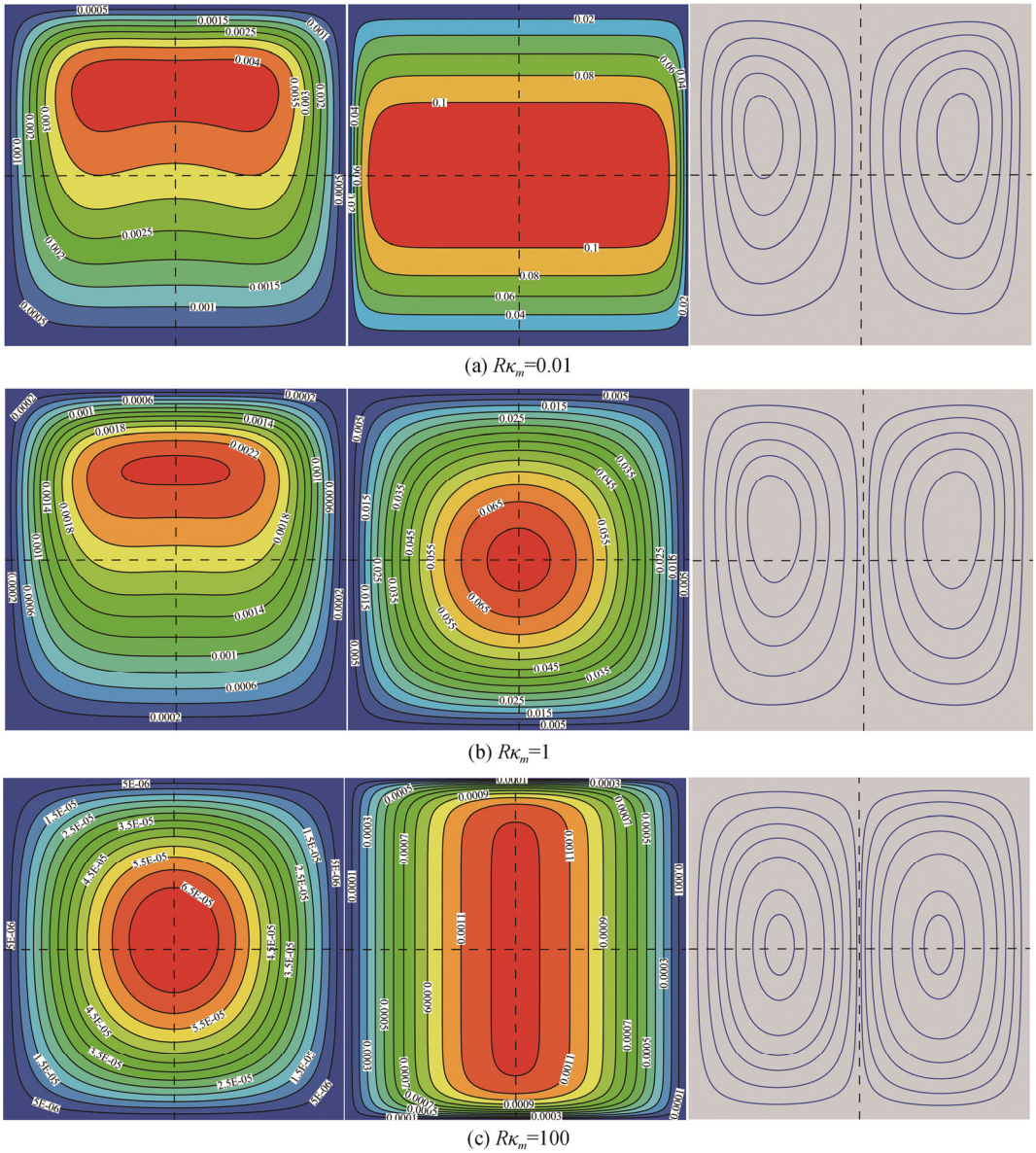

(a) $R\kappa_m$=0.01

(b) $R\kappa_m$=1

(c) $R\kappa_m$=100

Fig. 5 The influence of the thermal anisotropy: the streamlines (right) and temperature distribution of fluid (left) and solid matrix (middle) for different $R\kappa_m$

for $\theta_p = \pi/4$, due to higher permeability (K_1) at an angle of $\pi/4$ to the vertical axis, the non-symmetric nature of the vortices can be observed.

Fig. 5 illustrates the streamline and the temperature distribution for fluid and solid. The temperature distributions for both the fluid and solid decrease with the increase in thermal conductivity ratio. It should be noted that the thermal conductivity in vertical direction increases as $R\kappa_m$ increases, thus the overall thermal conductivity increases and the internal heat transfer will be enhanced. For a very large $R\kappa_m$ (i.e. $R\kappa_m$=100), the heat transfer will be dominated by conduction. And the influence of the convection is comparetively not as intense as conduction, so the centers of the eddies will move downward. Due to relatively larger thermal conductivity in the vertical direction, the temperature gradients for the interstitial fluid for $R\kappa_m$=100 is smaller than that for $R\kappa_m$=0.01 and 1. It can also be found that the direction with larger thermal conductivity (i.e. the horizontal direction in Fig. 5(a) and vertical direction in Fig. 5(c)) is the main direction for the heat transfer.

5. Conclusion

In the present paper, a multiple-relaxation-time (MRT) lattice Boltzmann (LB) method based on the assumption of local thermal non-equilibrium conditions (LTNE) is established to investigate the natural convective process

in a hydrodynamically and thermally anisotropic porous medium at the REV scale. Three sets of evolution equations are applied to solve the flow field based on the generalized non-Darcy model and the temperature fields of fluid and porous matrix under the LTNE conditions, respectively. The hydrodynamic anisotropy due to the porous media is considered by a permeability tensor and a Forchheimer coefficient tensor, while thermal anisotropy is accounted for with a heat conductivity tensor and a special relaxation matrix with some off-diagonal elements. Different from most of the existing Rev-LB models for porous media, where deviation term exists in the corresponding macroscopic equation, the presented model can recover the exact governing equations for natural convection under LTNE with anisotropic permeability and thermal conductivity with no deviation terms through the Chapman–Enskog procedure by selecting an appropriate equilibrium moments and discrete source terms accounting for the local thermal non-equilibrium effect, as well as choosing an off-diagonal relaxation matrix with some specific elements.

The presented MRT model is firstly validated by the numerical simulation of the natural convection problem in porous media with internal heat generating solid matrix where there exists simulating results reported in the literatures. From the numerical analysis and comparison, it can be found that good agreements can be achieved between the predicted results and the existing results. Finally, the proposed model is adopted to investigate the problem of natural convection in a hydrodynamically and thermally anisotropic porous medium under LTNE.

Acknowledgments

This work was supported by the National Natural Science Foundation of China (Grant No.51806067), China Postdoctoral Science Foundation (Granted No. 2015M572310), Fundamental Research Funds for the Central Universities (Granted No. 2017MS018), Guangdong Province Science and Technology projects (Grante 2017A040402005) and Guangdong Bureau of Quality and Technical Supervision Science and Technology projects (Granted No. 2016CT23).

References

[1] Minkowycz W.J., Haji-Sheikh A., Vafai K., On departure from local thermal equilibrium in porous media due to a rapidly changing heat source: the Sparrow number. International Journal of Heat and Mass Transfer, 1999, 42(18): 3373–3385.

[2] Baytas A.C., Thermal non-equilibrium natural convection in a square enclosure filled with a heat-generating solid phase, non-Darcy porous medium. International Journal of Energy Research, 2003, 27(10): 975–988.

[3] Nield D.A., Bejan A., Convection in porous media, 4th ed. Springer, New York, 2013.

[4] Guo Z., Zheng C.G., Theory and applications of lattice Boltzmann method. Science Press, Beijing, 2009. (in Chinese)

[5] Guo C., Nian X., Liu Y., et al., Analysis of 2D flow and heat transfer modeling in fracture of porous media. Journal of Thermal Science, 2017, 26(4): 331–338.

[6] Madejski P., Krakowska P., Habrat M., et al., Comprehensive approach for porous materials analysis using a dedicated preprocessing tool for mass and heat transfer modeling. Journal of Thermal Science, 2018, 27(5): 479–486.

[7] Guo Z., Zhao T.S., Lattice Boltzmann model for incompressible flows through porous media. Physical Review E, 2002, 66: 036304.

[8] Guo Z., Zhao T.S., A lattice Boltzmann model for convection heat transfer in porous media. Numerical Heat Transfer, Part B, 2005, 47(2): 157–177.

[9] Gao D., Chen Z., Lattice Boltzmann simulation of natural convection dominated melting in a rectangular cavity filled with porous media. International Journal of Thermal Sciences, 2011, 50(4): 493–501.

[10] Wang L., Mi J., Guo Z., A modified lattice Bhatnagar–Gross–Krook model for convection heat transfer in porous media. International Journal of Heat and Mass Transfer, 2016, 94: 269–291.

[11] Liu Q., He Y.L., Li Q., Tao W.Q., A multiple-relaxation-time lattice Boltzmann model for convection heat transfer in porous media. International Journal of Heat and Mass transfer, 2014, 73: 761–775.

[12] Hu Y., Li D., Shu S., Niu X., A multiple-relaxation-time lattice Boltzmann model for the flow and heat transfer in a hydrodynamically and thermally anisotropic porous medium. International Journal of Heat and Mass Transfer, 2017, 104: 544–558.

[13] Gao D., Chen Z., Chen L., A thermal lattice Boltzmann model for natural convection in porous media under local thermal non-equilibrium conditions. International Journal of Heat and Mass Transfer, 2014, 70: 979–989.

[14] Huang R., Wu H., A modified multiple-relaxation-time lattice Boltzmann model for convection–diffusion equation. Journal of Computational Physics, 2014, 274: 50–63.

[15] Guo Z., Zheng C.G., Shi B.C., An extrapolation method for boundary conditions in lattice Boltzmann method. Physics of Fluids, 2002, 14(6): 2007–2010.

[16] Tang G.H., Tao W.Q., He Y. L., Thermal boundary condition for the thermal lattice Boltzmann equation. Physical Review E, 2005, 72(1): 016703.